Polar curved polycyclic aromatic hydrocarbons in soot formation

Jacob W. Martin[a], Kimberly Bowal[a], Angiras Menon[a], Radomir I. Slavchov[a], Jethro Akroyd[a], Sebastian Mosbach[a], Markus Kraft[a,b,*]

[a]*Department of Chemical Engineering and Biotechnology, University of Cambridge, West Site, Philippa Fawcett Drive, Cambridge, CB3 0AS, United Kingdom*
[b]*School of Chemical and Biomedical Engineering, Nanyang Technological University, Singapore 637459*

Abstract

In this paper we consider the impact of polar curved polycyclic aromatic hydrocarbons (cPAH) on the process of soot formation by employing electronic structure calculations to determine the earliest onset of curvature integration and the binding energy of curved homodimers. The earliest onset of curvature integration was found to be a six ring PAH with at least one pentagonal ring. The σ bonding in the presence of pentagons led to curvature, however, the π bonding strongly favoured a planar geometry delaying the onset of curvature and therefore the onset of a flexoelectric dipole moment. The binding energies of cPAH dimers were found to be of similar magnitude to flat PAH for one to two pentagons with an alignment of the dipole moments vectors. For the more curved structures, steric effects reduced the dispersion interactions to significantly reduce the interaction energy compared with flat PAH. Homogeneous nucleation of cPAH at flame temperatures then appears unlikely, however, significant interactions are expected between chemi-ions and polar cPAH molecules suggesting heterogeneous nucleation should be explored.

Keywords:
Curved polycyclic aromatic hydrocarbons, Flexoelectric dipole, Soot formation, Combustion, Dimers

∗Supplementary Material is available for this paper.

Colloquium submitted for: Soot, Nanomaterials, and Large Molecules

Method of Determination: Method 2

Total Word Count: 2854 words

*Corresponding author
Email address: mk306@cam.ac.uk (Markus Kraft)

1. Introduction

Carbon particulate emissions from incomplete combustion of hydrocarbons in engines and open fires contributes to climate change [1, 2] and impacts human health [3]. Considerable efforts to understand and mitigate the formation of soot has led to an increased understanding of the gas phase chemistry and the dynamics of soot particles as they agglomerate. However, significant uncertainty remains around the transition from molecules into a solid particle [4]. Recent high resolution transmission electron microscopy (HRTEM) studies have shown that significant fractions of curved polycyclic aromatic hydrocarbons (cPAH) in soot [5, 6]. With the majority of fringes containing a single inflection point indicating pentagonal rings are present. Curvature analysis of the fringes using geometrical [5] and statistical models of the curvature [7] 28–49% of the fringes were determined to contain curvature indicating ≥1 pentagon. The range of pentagon integration was predicted to span 1–3 pentagons. Corannulene [8] and fullerenes [9] have also been synthesised in flames, so the presence of these curved fragments does not come as a surprise.

Once curvature is integrated, significant electric polarisation of the molecule occurs (flexoelectric effect) [10]. For the size of fragments found in primary soot particles determined from HRTEM and optical band gap methods (10-20 rings)[11] we predicted a range of 4–6.5 debye (which is two to three times that of water; 1.85 debye [12]) [10]. Figure 1 shows the electrostatic potential around coronene, corannulene and water. The quadrupolar potential of coronene with the negative potential, perpendicular to the molecule's plane, can be clearly seen and is due to the π-bonding. This becomes significantly polarised for corannulene, giving a dipole moment similar in magnitude to water 2.07 debye [13]. Homann suggested a nascent soot formation mechanism that involved homogeneous nucleation of cPAH which could be enhanced by the flexoelectric dipole-dipole interactions [14]. Heterogeneous ion-induced nucleation of nascent soot around chemi-ions has also been suggested for nascent soot formation which could be enhanced by ion-dipole interactions [15].

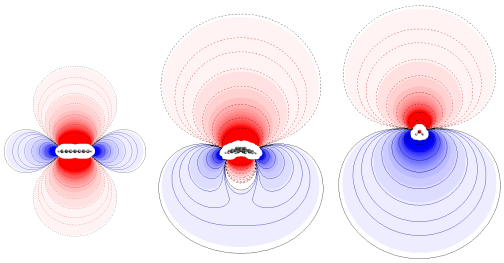

Figure 1: Cross section of the electric potential, (+) blue, (−) red, for coronene (left), corannulene (middle) and water (right).

In this paper we will outline begin by discussing the earliest onset of curvature integration, then calculate the binding energy between dimers of curved PAH to consider the case of homogeneous nucleation. The interaction between polar molecules, non-polar molecules and chemi-ions are then discussed as they relate to soot formation.

2. Methodology

The electronic structure calculations and geometry optimisations were performed using the Gaussian 09 software [16]. For the curvature integration calculations, the hybrid density functional theory (DFT) method B3LYP with the 6-311G(d,p) basis set was used, which has been found to provide structures for small curved aromatics to the quality of those determined from x-ray crystallography [17, 18]. We found this level of theory to provide molecular dipoles moments to within 6% error compared with experimentally measured dipole moments [10]. Care was taken to ensure that geometry optimisations provided a structure not at a saddle point geometry (e.g. small cPAH can invert through a planar transition state geometry [19]). C_1 symmetry was enforced for all structures, initial geometries were purposely curved away from planar and frequency calculations ensured no negative frequencies indicating a convex minima in the potential energy were found. For flat PAH (fPAH) dimerisation energies we have previously made use of symmetry-adapted perturbation theory DFT methods SAPT(DFT) which were found to reproduce the exfoliation energies of graphene [20]. In this case, the intermolecular potential energy was easily sampled by increasing the interplanar distance between the dimers and calculating the binding energy as a function of distance. However, for curved aromatic molecules a more complex geometry can result from the symmetry breaking of the curvature and full geometry-optimised structures were sought. This required a sufficiently rapid and scaleable method in order to optimise the geometry of the largest structures. We therefore made use of a hybrid DFT method with an empirical dispersion correction called B97D [21]. This method has been shown to produce binding energy to accuracies of CCSD(T) or SAPT(DFT) methods for two cPAH corannulene and sumanene [22, 23]. (See Supplementary Information for further details.)

3. Results and discussion

3.1. Curvature integration

We have previously found a direct relationship between the curvature of sp^2 hybridised carbon atoms (measured via pyramidalisation angle θ_p) and the local dipole moment in curved PAH (through the flexoelectric constant $f_{\theta p}$ = 2.24 D/rad). This pyramidalisation angle θ_p describes the amount of local curvature at each carbon atom and is constructed from a vector that makes equal angles with the three sigma bonds $\theta_{\sigma\pi}$ ($\theta_p = \theta_{\sigma\pi} - 90°$), which is used to describe when a structure becomes curved (when $\theta_p > 0$) (Fig. 2).

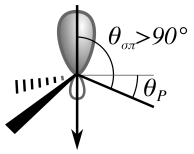

Figure 2: Schematic of the pyramidalisation angle and the definition of θ_P and the $\theta_{\sigma\pi}$ angle.

It is important to understand the onset of curvature integration in PAH formation in order to know when a significant flexoelectric dipole moment is expected during PAH formation in hydrocarbon flames. Various mechanisms for pentagon integration have been proposed, such as acetylene addition to fluoranthene [24], dehydrogenation of a five-member bay site [25, 26], oxidation of a zig-zag edge [27], dehydrogenation of aromers [14] or a C_1/C_2 mechanism [28]. Our goal here is not to comment on which mechanisms are of most importance, but to consider under which molecular geometries curvature is integrated and expand the structures explored in [10]. Figure 3 shows the various strategies employed.

The geometry of hexagonal and pentagonal nets should dictate that once two hexagonal rings border a pentagonal ring, curvature should be integrated. Considering the base structures, labelled **ac**, **fa**, **ph**, **be** and **1a** in Figure 3, no curvature is observed until the pentagon is entirely enclosed by five hexagonal rings. To understand the discrepancy between a geometrical nets and that found in the calculated structures, the bonding must be considered. The σ-bonding of the sp^2 aromatic network contributes to curvature integration by limiting the bond lengths (1.3–1.6 Å) and providing an angle potential optimal at 120°. The π-bonding network however resists bending (leading to a large elastic modulus of 21.5 eV/Å^2 [29]), which favours the planarisation of the molecules. The π-bonding dominates for two to four bordering hexagons with the bond lengths and angles changing to accommodate the planar structure. The planarisation is only overcome for the structure with a pentagon completely enclosed by hexagons **1a**.

We extended our previous set of structures that integrated curvature due to enclosed pentagons to include non-enclosed pentagons to determine other curved geometries via two methods: increasing the hexagonal aromatic network around the structure or by acetylene addition to zig-zag edge site, as suggested by Pope and Howard [24]. For structures **fa** and **ph** with a single pentagon and three bordering hexagons, additional hexagonal network growth did not give rise to curvature. However, for the structure **be** with four hexagonal rings enclosing the pentagonal ring, we found that hexagonal growth did lead to curvature and a flexoelectric dipole moment. However, substantial growth was required with initial addition of hexagonal aromatic rings to the left and right of the pentagonal ring not leading to curvature integration; hexagonal rings were required a further layer below the **be** molecule (as observed in the orientation in Figure 3). We also found that substantial curvature could be integrated for the geometry with two unenclosed pentagons joined by two hexagons (Figure 3 **cp**). An effective curvature integration mechanism was also found for the addition of acetylene to benzo(ghi)fluoranthene **be**. This rapidly increased the curvature (from $\theta_{p,max}$ = 6.8, 9.3, 10.5°) and dipole moment of these structures (from μ = 1.51, 2.45 to 3.03 debye). This was also explored for corannulene and a substantial dipole moment was found with these non-integrated pentagonal rings giving dipole moments of 2.93, 3.49, 3.96, 4.36 to 4.73 debye. The additional pentagonal ring integrated curvature more effectively due to its decreased internal angles compared with the hexagonal rings. This is further highlighted by comparing the curvature of pentacetylcorannulene **pa** and pentabenzocorannulene **pb**, the former was found to be more pyramidalised; $\theta_{p,max}$ = 12.3° compared with the latter $\theta_{p,max}$ = 9.2°. Acetylene additions to zig-zag sites – edge based peripheral pentagonal rings – are not persistent at high temperature and are prone to desorb, migrate or rearrange into hexagonal rings on zig-zag edges [25]. However, if further acetylene addition occurs enclosing the pentagonal ring by hexagonal rings would represent the most effective manner to integrate stable curvature, with the second most effective being acetylene addition to zig-zag edge site. Returning to the question of the critical size for the onset of curvature, Figure 4 shows the dipole moment as a function of ring size with the onset of curvature found to be 6 rings for the pentagon enclosure and acetyl curvature integration strategies. For the hexagonal extension strategy the onset of curvature was found to be at 10 rings.

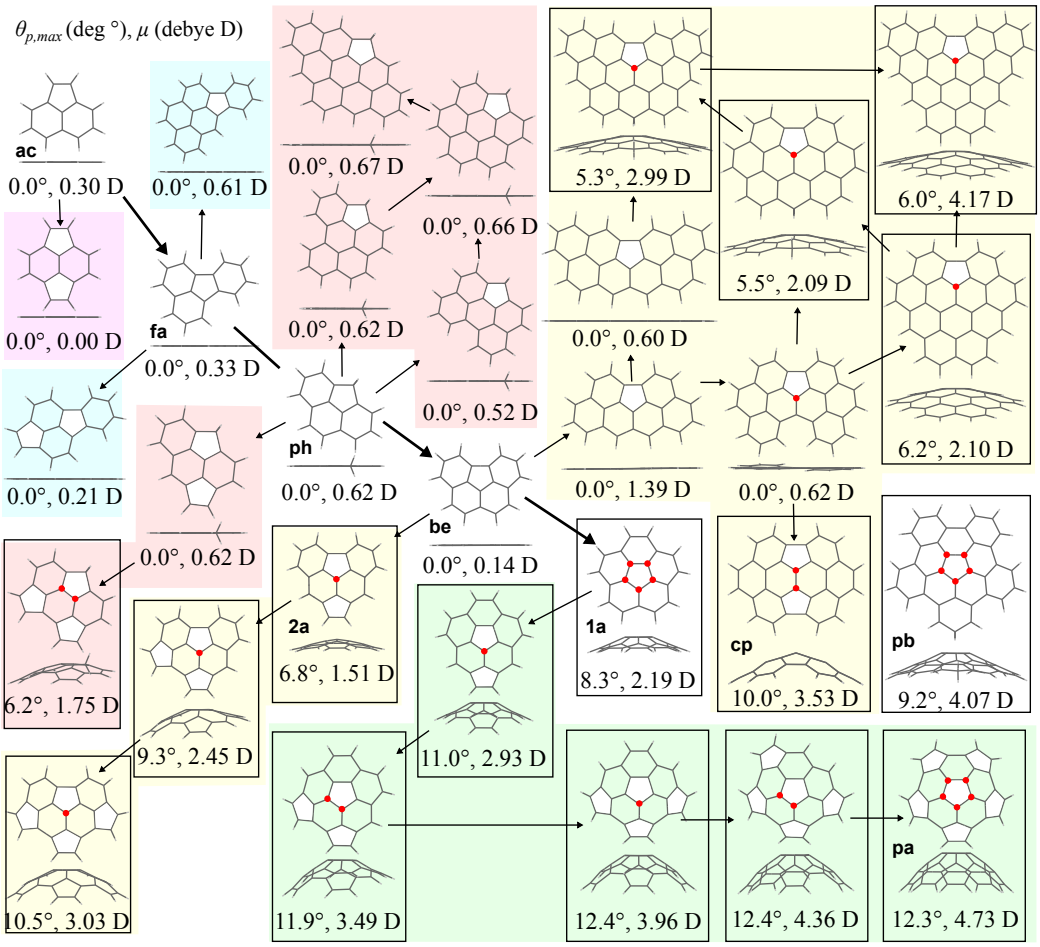

Figure 3: Optimised geometries are shown from above and side. The curved structures are framed by a black box. The most pyramidalised carbon atom of each structure is denoted by a red circle and its θ_P value is quoted underneath, along with the dipole moment calculated at the B3LYP/6-311G(d,p) level of theory. Base structures with single pentagons with two acenaphthylene **ac**, three fluoranthene **fa**, phenanthrindene **ph**, four benzo(ghi)fluoranthene **be** or five corannulene **1a** bordering hexagons are shown along the diagonal with hexagonal extension top right, and acetylene addition bottom left.

3.2. Interactions between cPAH

We will now consider the impact of the flexoelectric dipole moment on the dimerisation of curved aromatic dimers in the size range found in soot (4–20 rings) with the most persistent pericondensed species having pentagonal rings entirely enclosed by hexagons. The dimerisation energy has been used to consider the stability of clusters of flat PAH molecules previously [4, 30–32]. Figure 5 shows the various binding energies of curved aromatic homodimers compared with flat PAHs of pyrene, coronene, ovalene, hexabenzocoronene and circumcoronene taken from [31]. For structures containing one to two pentagonal rings, we found a similar binding energy compared with planar PAH. However, further increases in the number of pentagons decreased the binding energy compared with a flat PAH of a similar mass.

Corannulene and coronene are small PAH whose similar binding energies allowing the role of dispersion and dipole-dipole interactions to be deduced. SAPT(DFT) calculations show a reduced dispersion interaction between corannulene dimers of -136 kJ/mol [23] compared with -145 kJ/mol [33] for coronene. This is also seen in the greater intermolecular distance between the dimers of corannulene of 3.62 Å compared with 3.58 Å. The role of the dipole can be seen in the electrostatic contribution, which for corannulene is 22% of the attractive potential compared with 13% for coronene. We also observed a higher dipole moment for the dimers compared with the sum of the two static dipole mo-

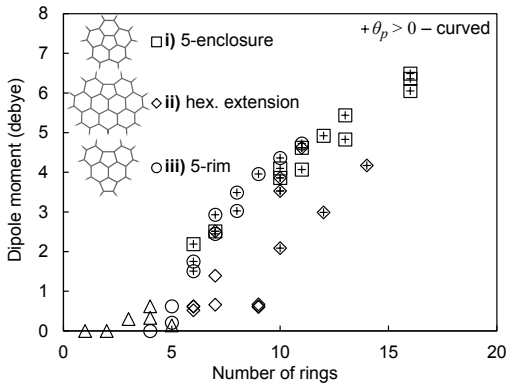

Figure 4: Dipole moment as a function of the number of rings for different curvature integration strategies. Curved structures are indicated by a plus symbol.

ments, indicating a small contribution from induction. SAPT(DFT) found induction to make up 4% of the attractive force in the case of corannulene [23]. (See the Supplementary Information for full details with comparisons to B97D simulations.)

While the dipole moment contributes to the binding energy, the molecule's curvature decreases the dispersion interactions due to steric effects. This can be seen from an increased intermolecular distance (see Supplementary Information) from 4.4–5 Å for one to three pentagons increasing to ~6-7 Å for four or more pentagons integrated. Due to the short range of the dispersion interactions (scaling as $\propto 1/r^6$) this increased distance significantly decreases the binding energy, most evidently for the structures with three or more pentagonal rings. For the highly strained structures a tilt was also found for the geometries. This is due to the positive hydrogen atoms interacting with the negative charge concentration around the carbon at the rim of the bowl and has been observed in crystal structure [34].

The similar binding energy of cPAH with one to two pentagonal rings to planar fPAH indicates that homogeneous nucleation of either species is unlikely to occur at flame temperatures [31]. Some preliminary molecular dynamics simulations have been performed on dimers **3c** by Chung and Violi [35] and a similar clustering behaviour was seen compared with planar fPAH. This is consistent with corannulene's sublimation temperature at standard conditions of 640 K [36]), which is similar to perylene 660 K at [37], a planar PAH with the same number of carbon atoms.

We have previously found that flat PAHs form stacked structures with strong dispersion interactions that are not significantly porous [38]. For species with greater than three pentagonal rings, significant decreases in the dispersion interactions could increase the porosity of soot. Soot with significant curvature, determined qualitatively from electron microscopy, was found to oxidise at lower temperatures than more graphitic soot, measured using thermal gravimetry, possibly indicating a more accessible structure [5, 39]. However, it is unclear whether this was primarily due to the increased porosity or an increased reactivity of curved structures due to the decrease in the aromaticity from the integration of non-hexagonal rings [40]. This decreased aromaticity provides a greater electron density to the carbon atoms around the rim of curved arenes and allows corannulene, for example, to perform aromatic substitution reactions as well as addition reactions (well known for the organic chemistry of buckybowls). Calculations comparing the oxidation pathway of pyrene and corannulene found significantly reduced activation barriers for corannulene [39]. Yet another oxidation mode could be direct attack of the pentagonal carbon atoms in curved PAH which we have previously explored in fullerenes [41].

3.3. Interactions between cPAH and other species

Permanent dipole-dipole interactions between cPAH and polar molecules provide small binding energies. Calculations have found significant interactions between water and corannulene with similar binding strengths to water dimers, -12.0 kJ/mol [42] compared with -13.2 kJ/mol [43] respectively (with water-graphite interaction energies of -9 kJ/mol reported [44]). These interactions are insignificant to nascent soot formation at flame temperatures.

The most significant interaction of cPAH with another species will be with charged species. Synthesised cPAHs such as corannulene **1a** are known to bind ions strongly (93–289 kJ/mol [45]). Anion binding is enhanced on the concave side by increased interaction with the positive hydrogen atoms and the increased dispersion interactions [46]. Cations can also bind to the concave face by interacting with the small amount of negative charge present (Figure 1), but most significantly they bind via dispersion interactions in this configuration [45]. Binding on the convex face favours binding above the pentagonal ring but can also strongly bond around the rim carbon atoms where charge is concentrated due to the C–H bond. Similar binding energies are found between curved and planar fPAHs [32, 45]. Curved aromatic molecules differ from planar fPAH in their capacity for ions due to the longer range of the interactions ($\propto -1/r^2$). This allows for corannulene to have increased capacity for lithium in battery applications (capacities of 372 and 602 mAh/g found for

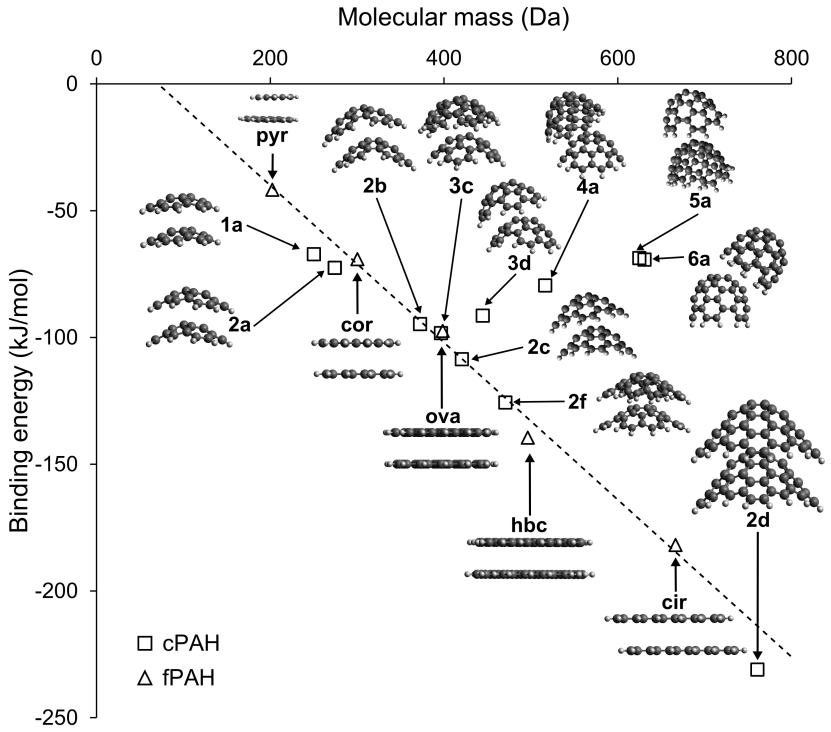

Figure 5: Binding energy of flat and curved PAH molecules as a function of molecular mass.

graphite and corannulene respectively [47]). Chen and Wang recently considered the stabilisation of clusters of fPAH bound to a chemi-ion. A sandwich complex was found to have significant binding energies - potentially enough for stabilisation at flame temperatures - however, addition of a third fPAH was weakly bound[32]. The binding energy of the curved PAH corannulene to alkali metal ions was found to be similar to that of the flat PAH coronene [45] but the longer range of the interactions indicate larger clusters could be stabilised. More calculations are required to further explore this possibility. Furthermore, significant experimental work is needed to determine the amount of curved PAH in soot formation to determine the possibility of an ion-induced nucleation mechanism in soot formation.

4. Conclusion

The earliest onset of curvature integration in PAH with pentagon integration was found for structures with greater than six rings with at least one pentagonal ring. Acetylene addition to a zig-zag edge was found to increase the curvature to a greater degree than hexagonal rings. Curvature integration is then understood as driven by the σ-bonding aromatic network while structure planarisation is due to π-bonding and is only overcome for structures with greater than six rings. The binding energy of curved PAH dimers with one or two pentagonal rings were found to be comparable with that of planar PAH molecules due to the contribution from the dipole moment. Steric effects reduce the dispersion interactions leading to structures with greater than three pentagons being significantly lower in binding energy than fPAH. Finally, the impact of curved PAH on other species and the role of polar aromatics interacting with chemi-ions was discussed.

Acknowledgments

This project is supported by the National Research Foundation (NRF), Prime Minister's Office, Singapore under its Campus for Research Excellence and Technological Enterprise (CREATE) programme.

References

[1] J. R. McConnell, R. Edwards, G. L. Kok, M. G. Flanner, C. S. Zender, E. S. Saltzman, J. R. Banta, D. R. Pasteris, M. M. Carter, J. D. W. Kahl, Science 317 (2007) 1381–1384.

[2] T. C. Bond, S. J. Doherty, D. W. Fahey, P. M. Forster, T. Berntsen, B. J. Deangelo, M. G. Flanner, S. Ghan, B. Kärcher, D. Koch, S. Kinne, Y. Kondo, P. K. Quinn, M. C. Sarofim, M. G. Schultz, M. Schulz, C. Venkataraman, H. Zhang, S. Zhang, N. Bellouin, S. K. Guttikunda, P. K. Hopke, M. Z. Jacobson, J. W. Kaiser, Z. Klimont, U. Lohmann, J. P. Schwarz, D. Shindell, T. Storelvmo, S. G. Warren, C. S. Zender, Journal of Geophysical Research Atmospheres 118 (2013) 5380–5552.

[3] P. J. Landrigan, R. Fuller, N. J. R. Acosta, O. Adeyi, R. Arnold, N. N. Basu, A. B. Baldé, R. Bertollini, S. Bose-O'Reilly, J. I. Boufford, P. N. Breysse, T. Chiles, C. Mahidol, A. M. Coll-Seck, M. L. Cropper, J. Fobil, V. Fuster, M. Greenstone, A. Haines, D. Hanrahan, D. Hunter, M. Khare, A. Krupnick, B. Lanphear, B. Lohani, K. Martin, K. V. Mathiasen, M. A. McTeer, C. J. L. Murray, J. D. Ndahimananjara, F. Perera, J. Potočnik, A. S. Preker, J. Ramesh, J. Rockström, C. Salinas, L. D. Samson, K. Sandilya, P. D. Sly, K. R. Smith, A. Steiner, R. B. Stewart, W. A. Suk, O. C. P. van Schayck, G. N. Yadama, K. Yumkella, M. Zhong, The Lancet (2017).

[4] H. Wang, Proceedings of the Combustion Institute 33 (2011) 41 – 67.

[5] D. Su, R. Jentoft, J.-O. Müller, D. Rothe, E. Jacob, C. Simpson, Ž. Tomović, K. Müllen, A. Messerer, U. Pöschl, R. Niessner, R. Schlögl, Catalysis Today 90 (2004) 127–132.

[6] M. L. Botero, D. Chen, S. González-Calera, D. Jefferson, M. Kraft, Carbon 96 (2016) 459–473.

[7] E. K. Yapp, C. G. Wells, J. Akroyd, S. Mosbach, R. Xu, M. Kraft, Combustion and Flame 176 (2017) 172–180.

[8] A. L. Lafleur, J. B. Howard, J. A. Marr, T. Yadav, The Journal of Physical Chemistry 97 (1993) 13539–13543.

[9] P. Gerhardt, S. Löffler, K. H. Homann, Chemical Physics Letters 137 (1987) 306–310.

[10] J. W. Martin, R. I. Slavchov, E. K. Y. Yapp, J. Akroyd, S. Mosbach, M. Kraft, The Journal of Physical Chemistry C 121 (2017) 27154–27163.

[11] M. L. Botero, E. M. Adkins, S. González-Calera, H. Miller, M. Kraft, Combustion and Flame 164 (2016) 250–258.

[12] S. L. Shostak, W. L. Ebenstein, J. S. Muenter, The Journal of Chemical Physics 94 (1991) 5875.

[13] F. J. Lovas, R. J. McMahon, J. U. Grabow, M. Schnell, J. Mack, L. T. Scott, R. L. Kuczkowski, Journal of the American Chemical Society 127 (2005) 4345–4349.

[14] K. H. Homann, Angewandte Chemie, International Edition in English 37 (1998) 2435–2451.

[15] H. F. Calcote, D. B. Olson, D. G. Keil, Energy & Fuels 2 (1988) 494–504.

[16] M. J. Frisch, G. W. Trucks, H. B. Schlegel, G. E. Scuseria, M. A. Robb, J. R. Cheeseman, G. Scalmani, V. Barone, G. A. Petersson, H. Nakatsuji, X. Li, M. Caricato, A. Marenich, J. Bloino, B. G. Janesko, R. Gomperts, B. Mennucci, H. P. Hratchian, J. V. Ortiz, A. F. Izmaylov, J. L. Sonnenberg, D. Williams-Young, F. Ding, F. Lipparini, F. Egidi, J. Goings, B. Peng, A. Petrone, T. Henderson, D. Ranasinghe, V. G. Zakrzewski, J. Gao, N. Rega, G. Zheng, W. Liang, M. Hada, M. Ehara, K. Toyota, R. Fukuda, J. Hasegawa, M. Ishida, T. Nakajima, Y. Honda, O. Kitao, H. Nakai, T. Vreven, K. Throssell, J. A. Montgomery, J. E. Peralta, F. Ogliaro, M. Bearpark, J. J. Heyd, E. Brothers, K. N. Kudin, V. N. Staroverov, T. Keith, R. Kobayashi, J. Normand, K. Raghavachari, A. Rendell, J. C. Burant, S. S. Iyengar, J. Tomasi, M. Cossi, J. M. Millam, M. Klene, C. Adamo, R. Cammi, J. W. Ochterski, R. L. Martin, K. Morokuma, O. Farkas, J. B. Foresman, D. J. Fox, Gaussian 09, Revision A 02, 2009.

[17] M. A. Petrukhina, K. W. Andreini, J. Mack, L. T. Scott, J. Org. Chem. 70 (2005) 5713–5716.

[18] S. Grabowsky, M. Weber, Y. S. Chen, D. Lentz, B. M. Schmidt, M. Hesse, P. Luger, Zeitschrift fur Naturforschung - Sect. B J. Chem. Sci. 65 (2010) 452–460.

[19] L. T. Scott, M. M. Hashemi, M. S. Bratcher, Journal of the American Chemical Society 114 (1992) 1920–1921.

[20] T. S. Totton, A. J. Misquitta, M. Kraft, The Journal of Physical Chemistry A 115 (2011) 13684–13693.

[21] S. Grimme, Journal of Computational Chemistry 27 (2006) 1787–1799.

[22] T. Janowski, P. Pulay, A. A. Sasith Karunarathna, A. Sygula, S. Saebø, Chemical Physics Letters 512 (2011) 155–160.

[23] E. M. Cabaleiro-Lago, B. Fernández, J. Rodríguez-Otero, Journal of Computational Chemistry (2017) 1–12.

[24] C. Pope, J. Marr, J. Howard, The Journal of Physical Chemistry 97 (1993) 11001–11013.

[25] R. Whitesides, M. Frenklach, The journal of physical chemistry. A 114 (2010) 689–703.

[26] R. Whitesides, M. Frenklach, Zeitschrift für Physikalische Chemie 229 (2015).

[27] R. Singh, M. Frenklach, Carbon 101 (2016) 203–212.

[28] X. Z. Wu, Y. R. Yao, M. M. Chen, H. R. Tian, J. Xiao, Y. Y. Xu, M. S. Lin, L. Abella, C. B. Tian, C.-L. Gao, Q. Zhang, S. Y. Xie, R. B. Huang, L. S. Zheng, Journal of the American Chemical Society 138 (2016) 9629–9633.

[29] I. Nikiforov, E. Dontsova, R. D. James, T. Dumitric, Physical Review B 89 (2014) 155437.

[30] J. H. Miller, W. G. Mallard, K. C. Smyth, The Journal of Physical Chemistry 88 (1984) 4963–4970.

[31] T. S. Totton, A. J. Misquitta, M. Kraft, Physical chemistry chemical physics 14 (2012) 4081–94.

[32] D. Chen, H. Wang, Energy & Fuels 31 (2017) 2345–2352.

[33] R. Podeszwa, The Journal of Chemical Physics 132 (2010) 044704.

[34] A. S. Filatov, L. T. Scott, M. A. Petrukhina, Crystal Growth & Design 10 (2010) 4607–4621.

[35] S.-H. Chung, A. Violi, Proceedings of the Combustion Institute 33 (2011) 693–700.

[36] J. S. Chickos, P. Webb, G. Nichols, T. Kiyobayashi, P.-C. Cheng, L. Scott, The Journal of Chemical Thermodynamics 34 (2002) 1195–1206.

[37] V. Oja, E. M. Suuberg, Journal of Chemical & Engineering Data 43 (1998) 486–492.

[38] P. Grančič, J. W. Martin, D. Chen, S. Mosbach, M. Kraft, Carbon 109 (2016) 608–615.

[39] A. Raj, S. Yeon, D. Cha, R. Tayouo, S. Ho, Combustion and Flame 160 (2013) 1812–1826.

[40] M. A. Dobrowolski, A. Ciesielski, M. K. Cyrański, Physical Chemistry Chemical Physics 13 (2011) 20557.

[41] J. W. Martin, G. J. McIntosh, R. Arul, R. N. Oosterbeek, M. Kraft, T. Söhnel, Carbon 125 (2017) 132–138.

[42] C. Pérez, A. L. Steber, A. M. Rijs, B. Temelso, G. C. Shields, J. C. Lopez, Z. Kisiel, M. Schnell, Phys. Chem. Chem. Phys. 19 (2017) 14214–14223.

[43] B. E. Rocher-Casterline, L. C. Ch'ng, A. K. Mollner, H. Reisler, The Journal of Chemical Physics 134 (2011) 211101.

[44] G. R. Jenness, K. D. Jordan, J. Phys. Chem. C 113 (2009) 10242–10248.

[45] R. C. Dunbar, The Journal of Physical Chemistry A 106 (2002) 9809–9819.

[46] H. Chen, W.-Y. Wang, L. Wang, C.-L. Zhu, X.-Y. Fang, Y.-Q. Qiu, Journal of Molecular Graphics and Modelling 64 (2016) 139–146.

[47] A. V. Zabula, A. S. Filatov, S. N. Spisak, A. Y. Rogachev, M. A. Petrukhina, Science 333 (2011) 1008–1011.

Supplementary Information

Additional comparison of the B97D functional to B3LYP and to SAPT(DFT) calculations are provided in the Supplementary Information.